(Received 19 August 2025, Accepted 27 November 2025, Scheduled 1 January 2026)

Research on Microstrip Array Antennas for Microwave De-Icing of Wind Turbine Blades

Yuchen Xia[1], Ning Liu[1,*], Zhengqing Yang[2], Yunhong Liu[1], Xianjun Sheng[1], Dongdong Zhang[1], Guangwen Jiang[3], and Xin Li[3]

[1] *School of Electrical Engineering, Dalian University of Technology, Dalian 116024, China*
[2] *School of Chemical Engineering, Dalian University of Technology, Dalian 116024, China*
[3] *China Resources New Energy Investment Co., Ltd., Suizhou Branch, Suizhou 441300, China*

ABSTRACT: Wind turbine blades are prone to icing in low-temperature environments, which affects the efficiency and safety of wind power generation. Microwave de-icing technology, with its high efficiency, non-contact, and rapid response characteristics, has become an important method for addressing the issue of blade icing. This paper focuses on the antenna design for a microwave de-icing system for wind turbine blades. Based on microstrip patch antennas, a low-side lobe, a high-gain array antenna was designed, operating at a frequency of 2.45 GHz with a maximum gain of 13.9 dB, with side lobe levels of −22.3 dB. An experimental system was established, and an infrared thermal imager was used to measure heating results, verifying temperature increases under different absorptive materials, heating times, heating powers, and radiation distances, laying the foundation for de-icing applications.

1. INTRODUCTION

As the global energy crisis and environmental issues continue to escalate, wind energy utilization has emerged as one of the most critical forms of renewable energy in the world today [1–3]. Approximately one-quarter of the world's wind turbines are located in cold regions [4], where they face severe icing issues [5]. Compared to warmer regions, colder environments have higher air density, and the available wind energy in cold climates can increase by approximately 10% [6]. Therefore, efficient de-icing technology for wind turbine blades is crucial for ensuring the safety and economic viability of wind power generation systems.

Currently, there is no mature, effective, and widely applicable de-icing technology for wind turbine blades. Existing methods include superhydrophobic material de-icing [7–9], hot air de-icing [10], electric heating de-icing [11], electric pulse de-icing, and ultrasonic de-icing [12]. Superhydrophobic materials are susceptible to vibration, radiation, and chemical corrosion, which can cause the hydrophobic layer to deteriorate [13]. Hot air de-icing can increase thermal resistance due to increased material thickness, requiring higher power output, which leads to increased energy consumption, blade weight gain, and reduced economic efficiency [14]. Electric heating film technology has high maintenance costs and is prone to damage from environmental factors [15]. Ultrasonic de-icing requires separate calibration for wind turbines from different manufacturers and models [16]. Electric pulse de-icing has limited coverage, making complete de-icing difficult and leaving significant residue [17].

Microwave heating, as an active de-icing method, has the advantages of uniform energy distribution, low energy consumption, easy maintenance, and immunity to lightning interference [18, 19]. General Electric (GE) established a microwave laboratory and conducted de-icing experiments using 2.45 GHz microwaves. In 2021, Luo et al. [20] developed a wind turbine blade de-icing device combining microwave and ultrasound, but it requires the turbine to be shut down for operation. Since icing primarily occurs at the blade tips in a confined space, this device leads to increased blade weight and additional vibration issues. Microstrip antennas have characteristics such as low profile, small size, light weight, and controllable beam direction, allowing them to be embedded within the blade to effectively reduce additional mass. In 2020, Yang et al. [21] designed a microwave directional heating system based on microstrip antennas, aiming to achieve directional heating in different regions of the cavity by controlling the microwave phase. In 2021, Li et al. [22] designed a multi-frequency multiplexed microstrip antenna, activating different antennas through frequency selection to control the heating region and heating effect.

This paper designs a high-gain, low-side-lobe microstrip array antenna. The microstrip antenna is tested in combination with actual absorptive coatings to verify the temperature rise under different absorptive materials, heating times, heating powers, and radiation distances.

2. BASIC THEORY

2.1. Principle of Microwave Heating

According to non-equilibrium thermodynamics, the thermal energy balance equation during the heating process is expressed

* Corresponding author: Ning Liu (liun@dlut.edu.cn).

as [23]:

$$\rho C_p \frac{dT}{dt} = \nabla \cdot (k \nabla T) + P_T \tag{1}$$

where ρ is the density of the medium, C_p the specific heat capacity of the medium, T the material temperature, t the heating time, k the thermal conductivity of the medium, and P_T the power density of the electromagnetic energy loss within the material, also known as the heating power. Furthermore, based on Maxwell's equations, the calculations under a harmonic alternating external field can be performed according to the following equations [16]:

$$P_T = 2\pi\varepsilon_0\varepsilon_r' f \tan\delta_\varepsilon E^2 + 2\pi\mu_0\mu_r' f \tan\delta_\mu H^2 \tag{2}$$

E is the electric field strength; f is the microwave frequency; H is the magnetic field strength; ε_0 represents the permittivity of free space; $\tan\delta_\varepsilon = \varepsilon_r''/\varepsilon_r'$ is the dielectric loss factor, where ε_r' and ε_r'' are the real and imaginary parts of the relative permittivity, respectively; μ_0 is the magnetic permeability of free space; μ_r' and μ_r'' are the real and imaginary parts of the relative complex magnetic permeability, respectively, where the former characterizes the ability of the material to store magnetic field energy, while the latter characterizes the ability to convert magnetic field energy into thermal energy. Moreover, $\tan\delta_\mu = \mu_r''/\mu_r'$ is defined as the magnetic loss factor, reflecting the attenuation of magnetic field energy in the material.

Equations (1) and (2) indicate that microwaves cause the temperature of the heated material to rise by inducing high-frequency oscillation of dipole molecules within the material, thereby generating "internal friction heat" [24].

2.2. Principle of Microwave De-Icing

The microwave de-icing process is essentially a de-icing technology based on electromagnetic wave heating. The blades are primarily composed of glass fiber and epoxy resin composite materials, which have a low dielectric loss tangent and poor microwave absorption capacity [25]. Microwaves penetrate the blade casing and directly act on the ice layer adhering to its surface. However, ice has a low microwave absorption rate, with a dielectric loss constant of approximately 0.001 compared to liquid water [26], resulting in low efficiency in absorbing microwave energy and converting it into thermal energy, thereby limiting the effectiveness of microwave de-icing [27, 28].

To improve microwave de-icing efficiency, an absorption coating with a high dielectric loss factor is applied to the blade surface, enabling it to effectively absorb microwaves and convert them into thermal energy, thereby enhancing its ability to heat ice layers. The principle is shown in Fig. 1, where the microwave absorption coating achieves efficient de-icing through radiative heating.

3. ANTENNA DESIGN

3.1. Array Antenna Design and Simulation

Feeding methods for microstrip array antennas include series feeding and parallel feeding. Parallel feeding results in significant transmission line losses. Considering the narrow layout

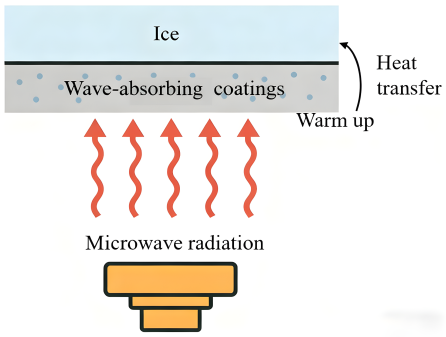

FIGURE 1. Microwave de-icing principle.

of the blade tips, a 1×8 series-fed antenna was designed to achieve high gain, low sidelobes, and compact dimensions. Its single feed line eliminates the need for a power-divider network, yielding a compact, low-loss design with minimal insertion loss [29]. Gain can be linearly increased by adding elements to achieve precise directivity.

The antenna is designed using an FR4 substrate with a dielectric constant $\varepsilon_r = 4.4$ and a thickness of $h = 2\,\text{mm}$. Electromagnetic simulation design was performed using CST, and the width W and length L of the individual rectangular patch elements are determined by the following equation [30].

$$W = \frac{1}{2f_r\sqrt{\mu_0\varepsilon_0}}\sqrt{\frac{2}{\varepsilon_r+1}} \tag{3}$$

$$L = \frac{1}{2f_r\sqrt{\varepsilon_{eff}}\sqrt{\mu_0\varepsilon_0}} - 0.824h\left(\frac{(\varepsilon_{eff}+0.3)(\frac{W}{h}+0.264)}{(\varepsilon_{eff}-0.258)(\frac{W}{h}+0.8)}\right) \tag{4}$$

where f_r is the resonant frequency, ε_r the dielectric constant of the substrate, and h the substrate thickness. When W/h is greater than 1, the effective dielectric constant can be calculated using the following formula [29]:

$$\varepsilon_{eff} = \frac{\varepsilon_r+1}{2} + \frac{\varepsilon_r-1}{2}\left[1+12\frac{h}{W}\right]^{-1/2} \tag{5}$$

In a series-fed microstrip antenna array, the width of each patch element is proportional to its equivalent admittance, which in turn is proportional to the input power of the patch element. The Taylor distribution achieves a balance between main lobe width and side lobe suppression by controlling the first n side lobes to have equal amplitudes and satisfy the specified side lobe level (SLL). By adjusting the width of each patch, the power amplitude of the excitation can be controlled, ensuring that the power distribution of the elements conforms to a Taylor distribution [31].

Assuming that the number of array elements is 8 and that the side lobe level is $-25\,\text{dB}$, the current excitation amplitude ratio of the array antenna based on the Taylor distribution is $W_1 : W_2 : W_3 : W_4 = 1 : 0.85 : 0.59 : 0.39$ [32]. To

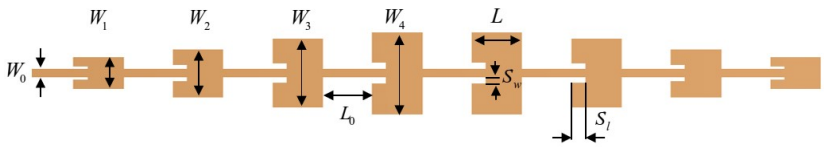

FIGURE 2. Antenna dimensions. The dimensions are ($W_1 = 13.4$, $W_2 = 18.5$, $W_3 = 29.0$, $W_4 = 36.3$, $L = 28.5$, $L_0 = 27.3$, $W_0 = 3.9$, $S_w = 2.3$, $S_l = 3$, (Units: mm)).

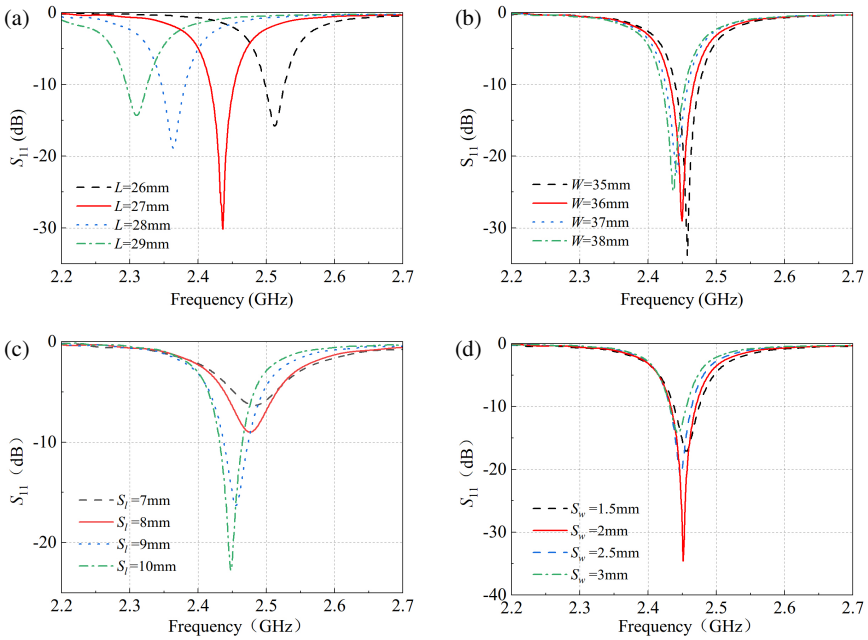

FIGURE 3. Parameter sweeps on antenna dimensions.

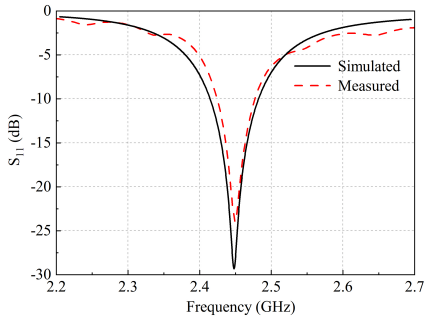

FIGURE 4. Return loss of the proposed antenna.

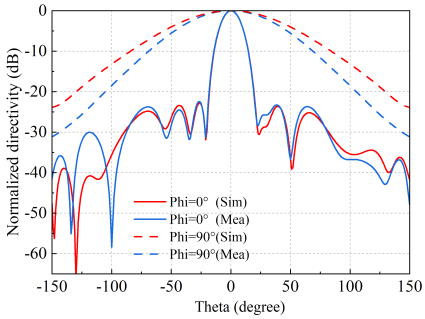

FIGURE 5. Normalized far-field of the antenna at 2.45 GHz.

increase bandwidth and facilitate impedance matching, an E-shaped patch series-fed antenna is adopted.

First, calculate W_1 and L_2 based on Equations (3) and (4). From the ratio, W_2 to W_4 can be derived. The method for calculating L is identical. The initial length $L_0 = \lambda_g/2$, and W_0 is the $50\,\Omega$ feeder width. The E-type patch antenna facilitates a reduction in feedline length.

The antenna dimensions are shown in Fig. 2, and the antenna is subjected to optimization analysis. As shown in Fig. 3, a parameter sweep analysis was conducted on the antenna width W, length L, insertion length S_l, and insertion width S_w. The W of the antenna unit has little effect on the resonance frequency of the antenna, while the L of the antenna unit has a significant impact. As L increases, the resonance frequency decreases. Changes in the S_w cause a slight shift in the resonance frequency, and as the S_l increases, the resonance frequency decreases.

The measured S_{11} and far-field radiation pattern of the fabricated antenna are shown in Fig. 4 and Fig. 5, respectively. The measured and simulated S_{11} values are both centered around 2.45 GHz. The measured gain of the directional pattern is 14.7 dB, which is 0.8 dB lower than the simulated value. The measured gain is 13.9 dB, and the directional pattern is basically consistent. The overall shape of the radiation pattern remains consistent with the simulation.

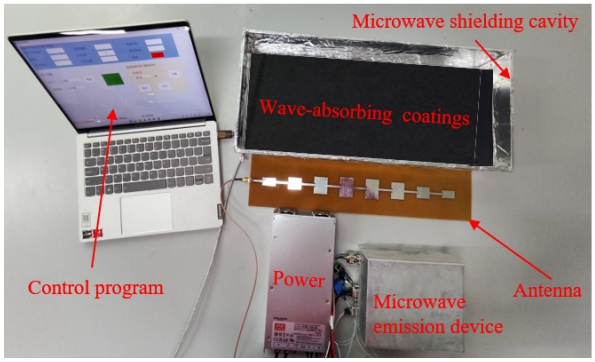

FIGURE 6. Experimental setup.

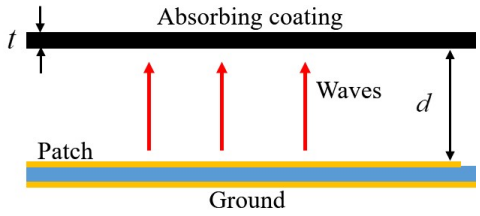

FIGURE 7. Radiation distance and angle.

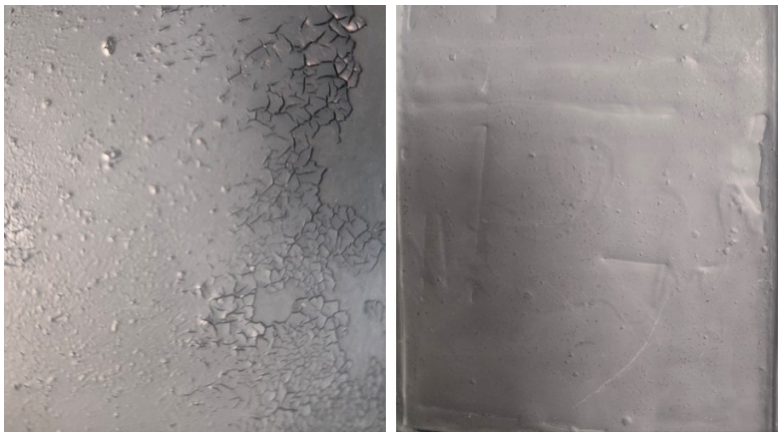

FIGURE 8. Absorbent coating.

4. MICROWAVE RADIATION HEATING EXPERIMENT

To verify the radiation heating performance of the antenna on the absorptive layer and prevent radiation to humans, the heating experiment of the wave-absorbing coating under microwave radiation is carried out in the metal shielding cavity,as shown in Fig. 6 used in the temperature measurement, the model of Fluke VT06.

The distance between the antenna and the coating is d, and they are placed parallel to each other and radiate vertically, as shown in Fig. 7. In Section 4.1, d remains at 60 mm.

As shown in Fig. 8, the carbon black and CNT/SiC absorptive coatings both have a concentration of 10%, and relative permittivities are 10 and 8.57, respectively and a thickness t of 0.3 mm.

4.1. Temperature Rise Experiments with Different Wave-Absorbing Coatings

The actual temperature rise measurement results are shown in Fig. 9 and Fig. 10.

As can be seen from Fig. 11, the temperature rise of the wave-absorbing coatings under the same radiation time condition is significantly enhanced with the increase in the input power. For example, at a radiation time of 30 min, the input power increases from 20 W to 50 W, corresponding to an increase in temperature rise from 15.6°C to 31.8°C, an increase of more than 100%. This trend indicates that the wave-absorbing coating exhibits stronger energy absorption and conversion capabilities under high-power microwave radiation, further demonstrating its potential advantages in microwave heating applications.

Under the same input power condition, the temperature rise shows an increasing trend with the growth of radiation time. Under the input power of 50 W, the temperature rise increases from 19.7°C at 10 min to 31.8°C at 30 min. In addition, the increase in temperature shows a certain nonlinear characteristic at different time stages, which is related to the material's wave absorption rate, specific heat capacity, and thermal radiation effect.

As can be seen from Fig. 12, under the same radiation time, the temperature increase and temperature increase rate of the carbon black coating are lower than those of the CNT/SiC composite coating. The temperature rise of the CNT/SiC composite coating is 31.8°C and that of the carbon black coating is 28°C under 30 min and 50 W conditions.

4.2. Warming Experiments with Different Microwave Radiation Distances

There is an inverse square decay relationship between the power density ρ of microwaves and the propagation distance d [33]. Therefore, when the radiation distance d increases, the energy density of microwaves reaching the surface of the coat-

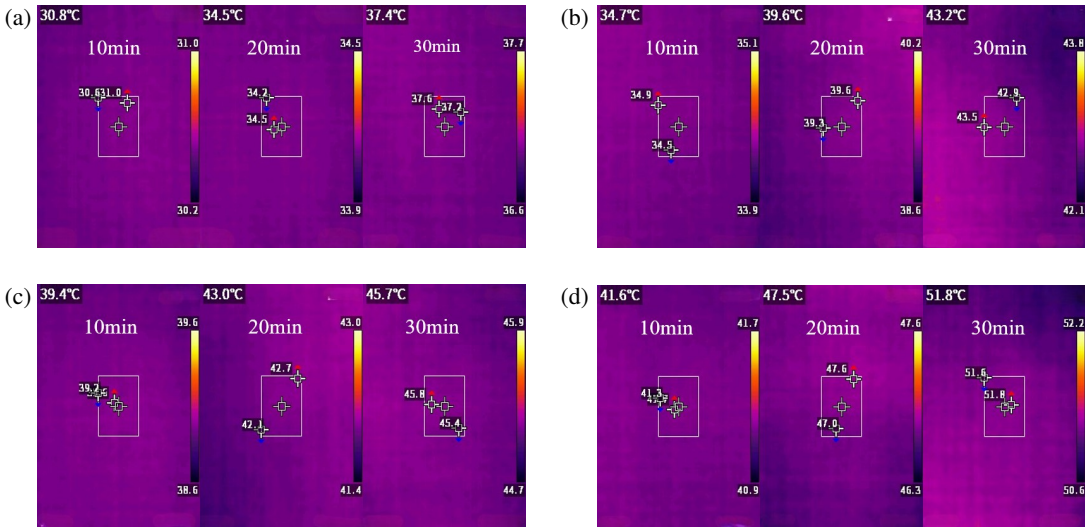

FIGURE 9. Temperature measurement results of CNT/SiC composite coating.

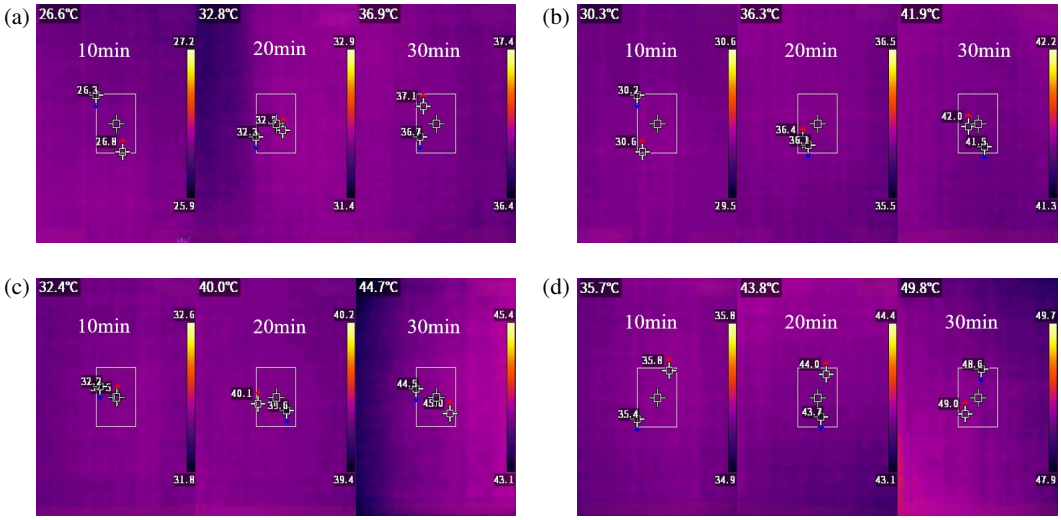

FIGURE 10. Temperature measurement results of carbon black composite coating.

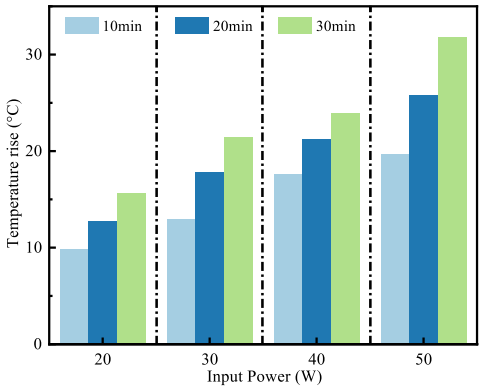

FIGURE 11. Temperature rise of CNT/SiC composite coatings.

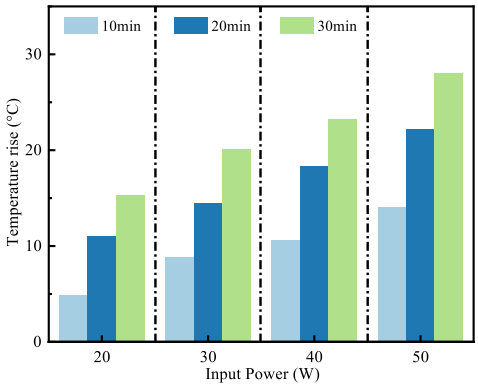

FIGURE 12. Temperature rise of carbon black coatings.

ing decreases significantly, and the absorbed energy decreases, thus reducing the rate of temperature rise.

The experimental results shown in Fig. 13 indicate that at short distances (30 mm), the microwaves mainly act on the coating by direct radiation, which makes the energy transfer more concentrated and efficiently heats the material. At a larger distance (90 mm), microwave may reduce the energy density due to scattering, bypassing and environmental losses, so that

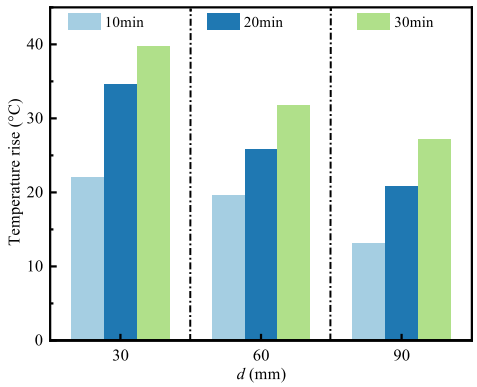

FIGURE 13. Temperature rise of CNT/SiC composite coatings with different microwave radiation distances.

the absorption efficiency of the coating decreases, and the temperature rise effect becomes poor. The electromagnetic waves radiated by the antenna are absorbed by the absorptive coating, which leads to heating the coating for 30 minutes.

5. CONCLUSION

In summary, this paper designs a microstrip array antenna for de-icing wind turbine blades, featuring high gain and low side lobes, combined with an absorptive coating. Experimental verification confirms the radiation effectiveness of the absorptive coating. Experimental results show that under the same radiation time conditions, the temperature rise of the absorptive coating significantly increases with increasing input power and decreases with increasing distance. Additionally, different absorptive coatings have varying effects on temperature rise.

Further experiments should be conducted within the blades, and phase-shifting techniques can be employed to achieve beam control. Additionally, due to the power capacity limitations of the dielectric substrate, the microwave de-icing antenna in this paper has certain limitations in terms of maximum power.

ACKNOWLEDGEMENT

This work was supported by the Commissioned R&D Project on Blade Microwave De-icing Technology (CRPR&D-LX-2023-019).

REFERENCES

[1] Tong, G., Y. Li, K. Tagawa, and F. Feng, "Effects of blade airfoil chord length and rotor diameter on aerodynamic performance of straight-bladed vertical axis wind turbines by numerical simulation," *Energy*, Vol. 265, 126325, 2023.

[2] Xu, Z., T. Zhang, Y. Lian, and F. Feng, "A parametric study on the effect of liquid water content and droplet median volume diameter on the ice distribution and anti-icing heat estimation of a wind turbine airfoil," *Results in Engineering*, Vol. 22, 102121, 2024.

[3] Meng, M., X. Zheng, Z. Wu, H. Hong, and L. Zhang, "Research and application of microwave microstrip transmission line-based icing detection methods for wind turbine blades," *Sensors*, Vol. 25, No. 3, 613, 2025.

[4] Li, Y., C. Sun, Y. Jiang, X. Yi, Z. Xu, and W. Guo, "Temperature effect on icing distribution near blade tip of large-scale horizontal-axis wind turbine by numerical simulation," *Advances in Mechanical Engineering*, Vol. 10, No. 11, 1687814018812247, 2018.

[5] Stoyanov, D. B., J. D. Nixon, and H. Sarlak, "Analysis of derating and anti-icing strategies for wind turbines in cold climates," *Applied Energy*, Vol. 288, 116610, 2021.

[6] Wallenius, T. and V. Lehtomäki, "Overview of cold climate wind energy: Challenges, solutions, and future needs," *Wiley Interdisciplinary Reviews: Energy and Environment*, Vol. 5, No. 2, 128–135, 2016.

[7] Wang, Y., Z. Huang, R. S. Gurney, and D. Liu, "Superhydrophobic and photocatalytic PDMS/TiO2 coatings with environmental stability and multifunctionality," *Colloids and Surfaces A: Physicochemical and Engineering Aspects*, Vol. 561, 101–108, 2019.

[8] Xu, K., J. Hu, X. Jiang, W. Meng, B. Lan, and L. Shu, "Anti-icing performance of hydrophobic silicone-acrylate resin coatings on wind blades," *Coatings*, Vol. 8, No. 4, 151, 2018.

[9] Peng, C., S. Xing, Z. Yuan, J. Xiao, C. Wang, and J. Zeng, "Preparation and anti-icing of superhydrophobic PVDF coating on a wind turbine blade," *Applied Surface Science*, Vol. 259, 764–768, 2012.

[10] Xie, T., J. Dong, H. Chen, Y. Jiang, and Y. Yao, "Experimental investigation of deicing characteristics using hot air as heat source," *Applied Thermal Engineering*, Vol. 107, 681–688, 2016.

[11] Li, X., H. Chi, Y. Li, Z. Xu, W. Guo, and F. Feng, "An experimental study on blade surface de-icing characteristics for wind turbines in rime ice condition by electro-thermal heating," *Coatings*, Vol. 14, No. 1, 94, 2024.

[12] Li, Y., H. Shen, and W. Guo, "Simulation and experimental study on the ultrasonic micro-vibration de-icing method for wind turbine blades," *Energies*, Vol. 14, No. 24, 8246, 2021.

[13] Zhang, Z., H. Zhang, X. Zhang, Q. Hu, and X. Jiang, "A review of wind turbine icing and anti/de-icing technologies," *Energies*, Vol. 17, No. 12, 2805, 2024.

[14] Madi, E., K. Pope, W. Huang, and T. Iqbal, "A review of integrating ice detection and mitigation for wind turbine blades," *Renewable and Sustainable Energy Reviews*, Vol. 103, 269–281, 2019.

[15] Daniliuk, V., Y. Xu, R. Liu, T. He, and X. Wang, "Ultrasonic de-icing of wind turbine blades: Performance comparison of perspective transducers," *Renewable Energy*, Vol. 145, 2005–2018, 2020.

[16] Huang, Q., Z. Yang, N. Liu, D. Zhang, G. Jiang, H. Zhang, H. Zhu, and X. Liu, "Research on the microwave heating and de-icing performance of various composite coatings," *Physica Scripta*, Vol. 100, No. 3, 035550, Feb. 2025.

[17] Petrenko, V. F., C. R. Sullivan, V. Kozlyuk, F. V. Petrenko, and V. Veerasamy, "Pulse electro-thermal de-icer (PETD)," *Cold Regions Science and Technology*, Vol. 65, No. 1, 70–78, 2011.

[18] Rawat, S., R. Samyal, R. Bedi, and A. K. Bagha, "Comparative performance of various susceptor materials and vertical cavity shapes for selective microwave hybrid heating (SMHH)," *Physica Scripta*, Vol. 97, No. 12, 125704, Nov. 2022.

[19] Singh, G., A. Bansal, H. Vasudev, and V. Mishra, "Sliding wear study of the Inconel-625 clad deposits by microwave heating on SS-304," *Physica Scripta*, Vol. 99, No. 6, 065503, May 2024.

[20] Luo, R., X. Chen, and J. Guo, "Design of deicing device for wind turbine blade based on microwave and ultrasonic wave," *Journal of Physics: Conference Series*, Vol. 1748, No. 6, 062018, 2021.

[21] Yang, Y., Z. Fan, T. Hong, M. Chen, X. Tang, J. He, X. Chen, C. Liu, H. Zhu, and K. Huang, "Design of microwave directional heating system based on phased-array antenna," *IEEE Transactions on Microwave Theory and Techniques*, Vol. 68, No. 11, 4896–4904, 2020.

[22] Li, C. N., X. Q. Lin, D. Y. Liu, and Z. Wen, "Regionally tunable microwave heating technology using time-frequency-space domain synthesis modulation method," *IEEE Transactions on Industrial Electronics*, Vol. 68, No. 10, 10 240–10 247, 2021.

[23] Vencels, J., M. Birjukovs, J. Kataja, and P. Råback, "Microwave heating of water in a rectangular waveguide: Validating EOF-Library against COMSOL multiphysics and existing numerical studies," *Case Studies in Thermal Engineering*, Vol. 15, 100530, 2019.

[24] Fan, S., Y. Wang, H. Wang, X. Zhang, Y. Zhu, J. Che, B. Sun, N. Yang, C. Yang, H. Xu, and C. Li, "Enhancing gas production from methane hydrate decomposition by microwave heating-induced: Modeling and experimental validation," *Energy*, Vol. 322, 135566, 2025.

[25] Hong, W., P. Xiao, H. Luo, and Z. Li, "Microwave axial dielectric properties of carbon fiber," *Scientific Reports*, Vol. 5, No. 1, 14927, 2015.

[26] Artemov, V., *The Electrodynamics of Water and Ice*, Vol. 124, Springer, 2021.

[27] El Khaled, D., N. Novas, J. A. Gazquez, and F. Manzano-Agugliaro, "Microwave dielectric heating: Applications on metals processing," *Renewable and Sustainable Energy Reviews*, Vol. 82, 2880–2892, 2018.

[28] Zhao, Y., Y. Chen, L. Tong, L. Zhong, and M. Jia, "The measurement on the dielectric properties of fresh-water ice with rectangular waveguide at 2.6 GHz–3.9 GHz," in *IGARSS 2008 — 2008 IEEE International Geoscience and Remote Sensing Symposium*, IV–1165–IV–1168, Boston, MA, USA, 2008.

[29] Lee, J., S. Park, J. Choi, W. Park, and K.-Y. Jung, "Compact series-fed microstrip patch array antenna in the 60 GHz band," *AEU — International Journal of Electronics and Communications*, Vol. 187, 155513, 2024.

[30] Jung, J., Y. Park, and J. Ryu, "Enhanced phase coherence in series-fed patch array antenna: A design method for uniform element spacing with low sidelobe levels," *Microwave and Optical Technology Letters*, Vol. 66, No. 12, e70066, 2024.

[31] Chen, Q., S. Yan, X. Guo, W. Wang, Z. Huang, L. Yang, Y. Li, and X. Liang, "A low sidelobe 77 GHz centre-fed microstrip patch array antenna," *IET Microwaves, Antennas & Propagation*, Vol. 17, No. 11, 887–896, 2023.

[32] Liu, J., N. Mu, F. Lv, H. Zhao, Q. Wang, and Y. Wang, "Low side lobe cylinder conformai omnidirectional millimeter wave microstrip antenna design," in *2016 46th European Microwave Conference (EuMC)*, 29–32, London, UK, 2016.

[33] Santos, T., M. A. Valente, J. Monteiro, J. Sousa, and L. C. Costa, "Electromagnetic and thermal history during microwave heating," *Applied Thermal Engineering*, Vol. 31, No. 16, 3255–3261, 2011.